Absence of Glial α-Dystrobrevin Causes Abnormalities of the Blood-Brain Barrier and Progressive Brain Edema*

Chun Fu Lien[‡]**, Sarajo Kumar Mohanta**[‡1]**, Malgorzata Frontczak-Baniewicz**[§]**, Jerome D. Swinny**[‡]**, Barbara Zablocka**[¶]**, and Dariusz C. Górecki**[‡2]

From the [‡]*Molecular Medicine, School of Pharmacy and Biomedical Sciences, University of Portsmouth, Portsmouth PO1 2DT, United Kingdom and the* [§]*Electron Microscopy and* [¶]*Molecular Biology Unit, Mossakowski Medical Research Centre, 02-106 Warsaw, Poland*

Background: Functional blood-brain barrier requires interactions between endothelia and astrocytes, but molecules involved in these contacts are not known.
Results: Absence of glial α-dystrobrevin protein causes leaky blood-brain barrier, water retention, and progressive brain edema.
Conclusion: Glial α-dystrobrevin is essential for endothelium-astrocyte interactions required for blood-brain barrier functions.
Significance: Pathologies altering α-dystrobrevin might lead to blood-brain barrier abnormalities.

The blood-brain barrier (BBB) plays a key role in maintaining brain functionality. Although mammalian BBB is formed by endothelial cells, its function requires interactions between endotheliocytes and glia. To understand the molecular mechanisms involved in these interactions is currently a major challenge. We show here that α-dystrobrevin (α-DB), a protein contributing to dystrophin-associated protein scaffolds in astrocytic endfeet, is essential for the formation and functioning of BBB. The absence of α-DB in null brains resulted in abnormal brain capillary permeability, progressively escalating brain edema, and damage of the neurovascular unit. Analyses *in situ* and in two-dimensional and three-dimensional *in vitro* models of BBB containing α-DB-null astrocytes demonstrated these abnormalities to be associated with loss of aquaporin-4 water and Kir4.1 potassium channels from glial endfeet, formation of intracellular vacuoles in α-DB-null astrocytes, and defects of the astrocyte-endothelial interactions. These caused deregulation of tight junction proteins in the endothelia. Importantly, α-DB but not dystrophins showed continuous expression throughout development in BBB models. Thus, α-DB emerges as a central organizer of dystrophin-associated protein in glial endfeet and a rare example of a glial protein with a role in maintaining BBB function. Its abnormalities might therefore lead to BBB dysfunction.

The blood-brain barrier (BBB)[3] has a crucial role in maintaining the specific microenvironment required for proper brain functioning. Although BBB relies on the properties of brain endothelial cells (BEC) (1, 2), recent studies indicate that BEC cooperate with pericytes, neurons, and astrocytes (3, 4) within functional "glio- and neurovascular units." These interactions shape the unique barrier properties and then regulate the cerebral blood flow and barrier performance (5). We now have a considerable knowledge of the molecular components of physical and metabolic barriers as well as the diverse transport systems controlling BBB permeability (1, 2).

In contrast, very little is known about the specific interactions between the endothelium and glia within gliovascular units. The astrocytic perivascular endfeet are closely apposed to the abluminal endothelial surface and are separated by but also cooperate in the formation and maintenance of the basement membrane composed of different extracellular matrix (ECM) proteins. Numerous observations indicate that both direct astrocyte interactions and astrocyte-derived factors are essential for the development and/or maintenance of BBB properties in BEC (2, 6, 7). However, our understanding of the exact molecules and mechanisms employed by astrocytes to influence BBB during ontogenic development and influence its maturation and permeability is far less comprehensive.

Matrix adhesion receptors, particularly dystroglycan (a dystrophin-associated protein, DAP) and the integrin families (8), are required for a proper interplay between ECM and cells. DAPs anchored via dystrophins are differentially expressed in BEC, neurons, and glia and show affinity for various ECM components (*e.g.* laminin and agrin) but also form heteromeric interactions with cell surface proteins (*e.g.* neurexins). Such multifunctionality is particularly applicable to complex interactions, such as those required at BBB. Indeed, the absence of DAP in dystrophic mouse brains results in BBB perturbations (9, 10).

We have previously demonstrated a highly specific subcellular distribution of α-dystrobrevin (α-DB), a dystrophin-related DAP member, in cells forming blood-tissue barriers and in glial

endfeet (11). Developmental expression of this protein coincides with the induction of specific differentiation processes, including the functional maturation of BBB (12). The α-dystrobrevin and its homologue β-DB show differential localization in the brain (13, 14). Dystrobrevins, by a complex network of interactions with DAPs, *e.g.* dystrophins and syntrophins, and with dysbindin, syncoilin, and β-synemin (desmuslin) provide anchorage for a further set of proteins, including various cytoskeleton components, receptors, and channels (15, 16). Although dystrophin absence causes disruption of the entire DAP complex, we have shown here that it is α-DB in glial endfeet that is essential for the formation and function of BBB. Its absence caused leaky blood vessels and progressively developing brain edema in α-DB-null (ADB) brains coinciding with abnormalities in astrocyte-BEC assembly involving dysregulation of specific DAPs, Kir4.1, and AQP4 channels. Thus, α-dystrobrevin emerges as a very rare example of a structural glial protein crucial for endothelial BBB functioning.

EXPERIMENTAL PROCEDURES

Animals—Adult C57Bl/6 control, mdx$^{\beta geo}$ (10) dystrophin-null, and α-dystrobrevin knock-out (ADB) mice were used (17). Animals were maintained in a 12-h light/dark cycle and fed normal diet and water *ad libitum*. All procedures were performed with permission of the local Animal Health and Welfare Committees and in accordance with the United Kingdom Home Office guidelines.

Antibodies—α-Dystrobrevin (α-DB) antibodies have been described previously (11, 12). Mouse anti-α-DB (clone 23; BD Biosciences), rabbit anti-α-DB-1 (α1-CTFP; gift from D. J. Blake), rabbit anti-α/β-dystrobrevin (gift from T. C. Petrucci), mouse anti-α-dystroglycan (clone VIA4-1; Millipore), mouse anti-β-dystroglycan (MANDAG2; Developmental Studies Hybridoma Bank (DSHB)), mouse anti-dystrophin (MANDRA1; DSHB), mouse anti-utrophin (MANCHO3; DSHB), mouse anti-syntrophin (clone 1351; Affinity BioReagents), rabbit anti-aquaporin-4 (AB2218, Millipore and AQP-004, Alomone Labs), rabbit anti-Kir4.1 (Alomone Labs), rabbit anti-laminin (Sigma), rabbit anti-glial fibrillary acidic protein (GFAP; Abcam), rabbit anti-occludin and rabbit anti-ZO-1 (Life Technologies), and rabbit anti-actin (Sigma-Aldrich) were also used. For permeability studies, rabbit anti-fibrinogen (Calbiochem), rabbit anti-albumin (Dako), and Cy3-conjugated donkey anti-mouse IgG (Fab fragment; Jackson ImmunoResearch Laboratories) were used. DyLight595/Fluorescein-conjugated GS-IB$_4$ isolectin (Vector Laboratories) were used as endothelial markers.

Blood-Brain Barrier Permeability Study—3-month-old mice were either injected with 4% Evans blue in saline (0.1 ml/10 g of body weight) intraperitoneally or anesthetized and injected intracardially. Following the dye circulation period, mice were perfused with phosphate-buffered saline (PBS; pH 7.4) and 4% paraformaldehyde and 15% saturated picric acid in 1× PBS, and brains were post-fixed at 4 °C overnight using the same fixative. Brains from nonperfused mice were also analyzed for comparison (18). 50–100-μm-thick vibratome sections were cut (VT1000S Leica), fixed, and either analyzed for Evans blue fluorescence or stained for fibrinogen, albumin, and IgG, as described below. Morphometric analyses of immunoreactive

blood vessels were performed using AxioVision Release 4.6 software (Axio Imager, Carl Zeiss), as described (19, 20). Random areas of confocal images were acquired, and the numbers of immunoreactive blood vessels within the area were counted. Statistical analysis was done with the OriginPro 8.1 software (Northampton, MA) using one-way analysis of variance followed by Tukey's or Games-Howell post hoc test. All measurements were expressed as means ± S.E. p values < 0.05 were considered as significant.

Brain Water Content Measurement—3-month-old mice were killed, and their brains were rapidly removed. Isolated hemispheres were weighed (wet mass) and then dried in a vacuum oven (VT6025; Thermo Fisher Scientific) for 24 h at 80 °C and −1,000 mbar, and the percentage of brain water content was calculated: (wet mass − dry mass) × 100/(wet mass) as described (21).

Cell Co-culture in Vitro Models—Postnatal day 0–2 brains from ADB or wild-type mouse pups were isolated, and meninges were carefully removed (22). Cerebral cortices were dissected and dissociated in Dulbecco's modified Eagle's medium (DMEM) containing 0.25% trypsin (Sigma-Aldrich) and 1 mg/ml DNase 1 (Roche Applied Science) for 1 h with gentle agitation. Dissociated tissue was washed three times in the astroglia culture medium (DMEM containing 2 mM L-glutamine, 20% fetal bovine serum (FBS), 100 units/ml penicillin, and 0.1 mg/ml streptomycin) before plating into culture flasks. Astrocytes were cultured in this medium for 8–10 days at 37 °C with 10% CO_2. Confluent cultures were shaken at 200 rpm for 2 days at 37 °C/10% CO_2 to dislodge contaminating microglia and oligodendrocytes (23–25). Astrocytes were passaged using cell dissociation solution (Sigma-Aldrich) and used no later than at passage 2. The bEnd3 immortalized mouse brain endothelial cells (26, 27) obtained from European Collection of Cell Cultures (ECACC) were cultured in the endothelial culture medium (DMEM supplemented with 2 mM L-glutamine, 10% FBS, 5 μM 2-mercaptoethanol, 1 mM sodium pyruvate, 1% nonessential amino acids, 100 units/ml penicillin, and 0.1 mg/ml streptomycin) at 37 °C with 5% CO_2. Only bEnd3 cells from passages 31–35 were used for this study. All culture media were changed every 3 days. For laminin-induced clustering, cells were treated for 24 h with 20 or 40 nM laminin-1 (L2020; Sigma-Aldrich) (28).

For two-dimensional cultures, ADB/wild-type cortical astrocytes were seeded into 25-cm² culture flasks or on coverslips and grown in the astroglia medium and in some cases with added 1 mM dBcAMP and 1% horse serum (29). After establishing a glial monolayer bed, 1×10^5 bEnd3 cells were added and grown in the endothelial medium. BBB co-cultures were kept at 37 °C with 5% CO_2 and analyzed at 0 (+2 h), 1, 2, 4, 6, and 8 days. Bright-field images were acquired using a ColorView II digital camera mounted on the IX71 inverted microscope (Olympus). Morphometric measurements of the length and area of glial columns were taken using its integrated analySIS software (Olympus).

Three-dimensional co-cultures were prepared as described (30–32), with few modifications. Briefly, ADB or wild-type cortical astrocytes and bEnd3 cells were pooled in DMEM to obtain a combined density of 1×10^6 cells/ml (1:1 astrocyte:

endothelial cells ratio). Cells were gently spun down (5 min at 1,000 rpm) to replace DMEM with 4 mg/ml Matrigel^{TM} (BD Biosciences) in the endothelial culture medium. Droplets of the Matrigel^{TM} dual-cell suspension were spotted into a 6-well plate and solidified for 15 min at 37 °C. These droplets were overlaid with the endothelial culture medium and incubated at 37 °C with 5% CO_2 for a week. Droplets were then detached, cryo-sectioned (cryostat CM3050 S, Leica), and immuno-stained as described below.

ECIS Monitoring of Blood-Brain Barrier Formation—ECIS® arrays (8W10E+; 8-well chambers, Applied Biophysics) were prepared and used as described before (33). 2×10^5 primary astrocytes/cm^2 (isolated as described above) were seeded into each chamber and maintained for 7 days in astroglial culture medium until monolayer was established. For electrode coating with endogenous extracellular matrix (34), astrocytes were lysed sequentially in sterile water (30 min at 37 °C), 1% Nonidet-P40 (5 min at 37 °C) followed by 1% Nonidet-P40 and 1% sodium deoxycholate in sterile water for 1 min at room temperature. Subsequently, 2×10^5 bEnd3 cells/cm^2 were seeded into each chamber containing either live wild-type/ADB astrocytes (direct cell-cell contact) or their respective ECM and cultured in endothelial culture medium. Barrier integrity and cell resistance were monitored at 2,000-Hz frequency using ECIS Zθ (Applied Biophysics) for 168 h at 37 °C with 5% CO_2.

Immunolocalization and Fluorescence Confocal Imaging—Vibratome sections or cell cultures were post-fixed with 4% paraformaldehyde in $1 \times$ PBS on ice for 30 min. Samples were blocked in 10% normal donkey serum (Biosera) in $1 \times$ PBS containing 0.5% Triton X-100 (PBST) for 3 h and incubated overnight at 4 °C with specific antibodies (see above). In some cases, 10 μg/ml DyLight 594/fluorescein-conjugated GS-IB$_4$ isolectin (Vector Laboratories) was used to visualize brain endothelial cells. Secondary antibody incubation was with 8 μg/ml Alexa Fluor 488-conjugated goat anti-rabbit IgG, 8 μg/ml Alexa Fluor 594-conjugated goat anti-rabbit IgG (Fab^2 fragment; Life Technologies), or 6 μg/ml Cy3-conjugated donkey anti-mouse IgG (monovalent Fab fragment; Jackson ImmunoResearch Laboratories). 5 μg/ml Hoechst 33342 (Life Technologies) was used for nuclear counterstaining. After each incubation step, samples were washed three times in PBST for 10 min. Samples were mounted in FluorPreserve^{TM} anti-fading reagent (Calbiochem), and sections were examined with a confocal laser-scanning microscope (LSM710; Zeiss, Oberkochen, Germany) using either a Plan Apochromatic 63$\times$ differential interference contrast oil objective (NA1.4) or a Plan Apochromatic 100$\times$ differential interference contrast oil objective (NA1.46). Z-stacks were used for routine evaluation of the labeling. All images represent a single optical section. Images from wild-type (WT) and ADB tissue sections were acquired under identical microscope settings using sequential acquisition of the different channels to avoid cross-talk between fluorophores. The pinholes for each channel were adjusted to one airy unit. All images were processed identically using the software Zen2009 Light Edition (Zeiss). Only brightness and contrast were adjusted for the whole frame, and no part of a frame was enhanced or modified in any way. Images were exported into Adobe Photoshop for figure arrangement. In negative controls,

primary antibodies were omitted, whereas the rest of the procedure was done exactly as described.

Transmission Electron Microscopy—Perfused brains were fixed in 4% paraformaldehyde and 15% saturated picric acid in $1 \times$ PBS at 4 °C for 24 h and postfixed in a mixture of 1% osmium tetroxide (OsO_4), 0.8% potassium ferricyanide $K_4[Fe(CN)_6]$, and the material was processed for transmission electron microscopy using standard protocols and analyzed in JEM 1011 (JEOL).

Histological Staining—Perfusion-fixed brains (as described above) from 18-month-old wild-type/ADB mice were processed into paraffin and sectioned (5 μm) using RM2235 microtome (Leica). Sections were deparaffinized and incubated in hematoxylin QS (H-3404; Vector Laboratories) and then in alcoholic eosin Y (Sigma-Aldrich) for 5 min each. Sections were differentiated, dehydrated in graded series of ethanol, and mounted in dibutyl phthalate xylene (DPX).

Protein Extraction, SDS-PAGE, and Blue Native Analysis—Brains or cells were homogenized in ice-cold lysis buffer containing 0.15 M sodium chloride, 50 mM sodium fluoride, 10 mM HEPES (pH 7.5), 5 mM EGTA, 5 mM EDTA, 1% Triton X-100 and protease inhibitors 2 mM sodium orthovanadate, 1 mM PMSF, 1 mM Pefabloc, 1 mM benzamidine, and 10 μg/ml aprotinin, and Complete^{TM} mini inhibitor mixture tablet (Roche Applied Science). After incubation on ice for 30 min on a shaking platform, the homogenates were centrifuged at $200 \times g$ for 5 min at 4 °C. Protein supernatants were collected and quantified using the bicinchoninic acid kit (Sigma-Aldrich). For SDS-PAGE, solubilized proteins (30 μg) were mixed with Laemmli sample buffer (Bio-Rad) and 2.5% β-mercaptoethanol, heated to 95 °C for 5 min, separated on 8–10% SDS-polyacrylamide gels, and electroblotted onto Hybond-P PVDF membranes (GE Healthcare).

Blue native analyses were performed according to Ref. 35. Brains were homogenized in ice-cold lysis buffer containing 0.32 M sucrose, 50 mM HEPES (pH 7.5), 2 mM EDTA and protease inhibitors 2 mM sodium orthovanadate, 1 mM PMSF, 1 mM benzamidine, and Complete^{TM} mini inhibitor mixture tablet (Roche Applied Science). After 1 h of incubation on ice, the homogenates were centrifuged at $1,000 \times g$ for 15 min at 4 °C to remove the nuclear pellets. Supernatants were further centrifuged at $164,000 \times g$ for 30 min at 4 °C using ultracentrifuge (XL-90; Beckman Coulter) with Ti70.1 rotor, and the crude membrane pellets were resuspended in the same lysis buffer but without sucrose. Cells were lysed in $1 \times$ NativePAGE sample buffer supplemented with 1% dodecyl-β-D-maltoside (Life Technologies) for 15 min on ice. The lysates were centrifuged at $23,000 \times g$ for 30 min at 4 °C. Protein samples were quantified using the bicinchoninic acid kit (Sigma-Aldrich). Solubilized proteins (20 μg) were mixed with Coomassie Blue G-250 (4:1), resolved on NativePAGE Novex 3–12% Bis-Tris gels (Life Technologies) alongside a molecular weight ladder Native-MARK (LC0725; Life Technologies), and electroblotted onto Hybond-P PVDF membranes (GE Healthcare).

Immunoblotting—All blots were incubated with a blocking solution containing 5% non-fat milk powder in PBST ($1 \times$ PBS/ 0.05% Tween 20) for 1 h at room temperature and incubated with a specific antibody in the same blocking solution overnight
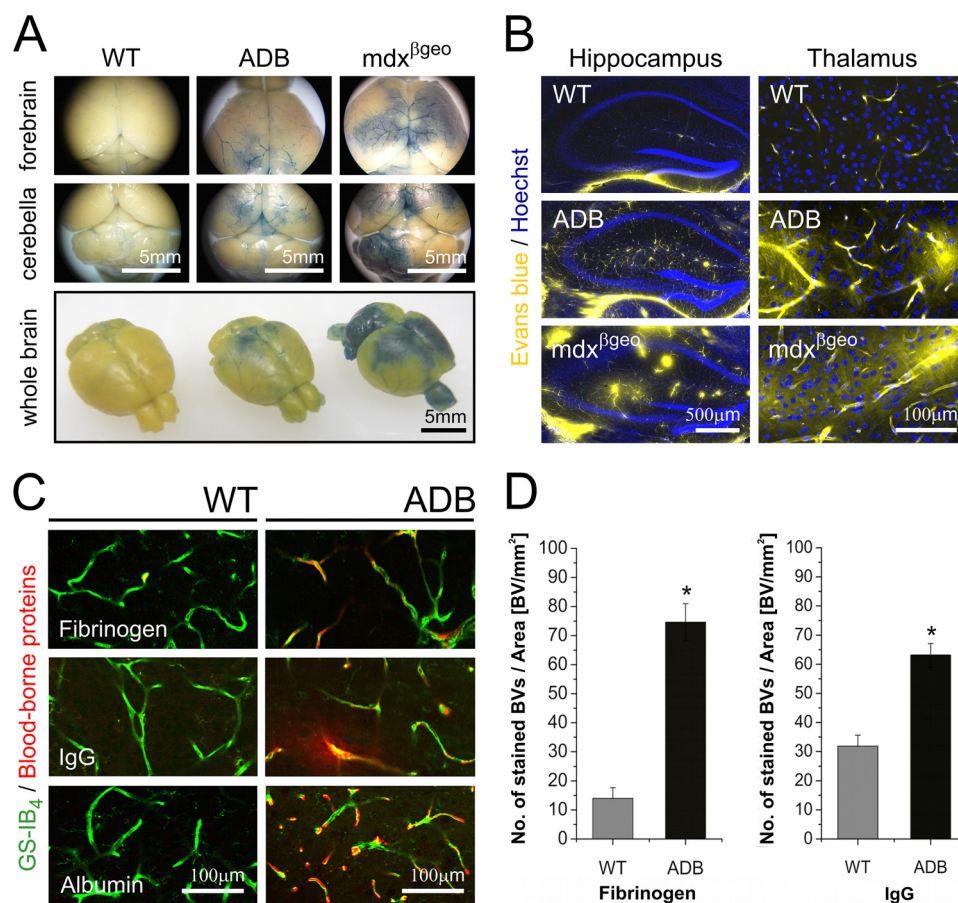
FIGURE 1. **Leaky BBB in α-dystrobrevin knock-out (ADB) brains.** *A*, macroscopic views of wild-type, ADB, and mdx[βgeo] (positive control) brains showing Evans blue extravasation in specific brain areas. *B*, confocal micrographs showing Evans blue extravasations (*yellow fluorescence*) into the parenchyma of ADB and mdx[βgeo] brains. *C*, confocal micrographs of blood vessels in the wild-type and ADB brain cortices stained for fibrinogen (*top*), IgG (*middle*), and albumin (*bottom*). Immunoreactivity for these blood components (*red*) is present outside the GS-IB$_4$-labeled (*green*) blood vessels. *D*, quantitative evaluation of fibrinogen and IgG immunoreactivities expressed as number of positive blood vessels (*BVs*) per area (mm^2) of cortex showed highly statistically significant differences (*, $p < 0.001$) between wild-type and ADB brains. *Error bars* represent ± S.E.

at 4 °C. Following three washes with PBST, membranes were incubated with appropriate horseradish peroxidase-conjugated goat anti-rabbit IgG or goat anti-mouse IgG (1:5,000, Sigma-Aldrich) at room temperature for 1 h, and signal was visualized using the UptiLight HS chemiluminescence substrate kit (Cheshire Sciences) and G:BOX Chemi XT 16 gel imaging system (Syngene). For negative controls, primary antibodies were omitted, and the rest of the protocol was performed as described above.

Statistical Analysis—was done with the OriginPro 8.1 software using one-way analysis of variance followed by Tukey's post hoc test. All measurements were expressed as means ± S.E. *p* value < 0.001 was considered as highly significant.

RESULTS

Leaky BBB in α-Dystrobrevin Knock-out Brains—To investigate the impact of α-DB absence on BBB integrity and function, we compared numbers of blood vessels showing the Evans blue extravasation and blood protein leakage into the brain tissues in WT and ADB mice. There were few blood vessels with detectable Evans blue, fibrinogen, albumin, or IgG staining around or outside the capillary lumen in the wild-type brains. In contrast, analysis of ADB brains showed abundant perivascular extravasations of both injected Evans blue and blood-borne proteins

into the brain. Mdx[βgeo] brains used as a positive control (10) confirmed BBB permeability (Fig. 1). Detailed morphometric analyses (19, 20) of vessels leaky for fibrinogen and IgG showed a highly statistically significant ($p < 0.001$) increase in numbers of such events in ADB brains (Fig. 1D).

Abnormalities in Endothelia-Glia Interactions Caused by the Absence of α-Dystrobrevin in Astrocytes—To dissect the mechanism(s) responsible for the leaky BBB in the absence of α-DB, two- and three-dimensional co-culture systems were used. Such systems, involving the interaction of just BEC and astrocytes from normal or ADB mice, allow for direct comparisons of changes in molecular interplay between BEC and glia caused by the absence of α-DB. As described (36), BEC added to confluent cultures of astrocytes penetrated under the astrocytic monolayer and caused its rearrangement into glial islands interconnected by thick multicellular glial columns. With time, the size of the islands decreased, whereas the columns elongated and the complexity of this network of columns increased (Fig. 2A). In the presence of wild-type astrocytes, such arrangements were highly reproducible and persisted for over 2 weeks in culture. However, when ADB glia was used, this glial lattice framework was significantly less complex, and the columns were thinner and fragile, with many discontinuities appearing
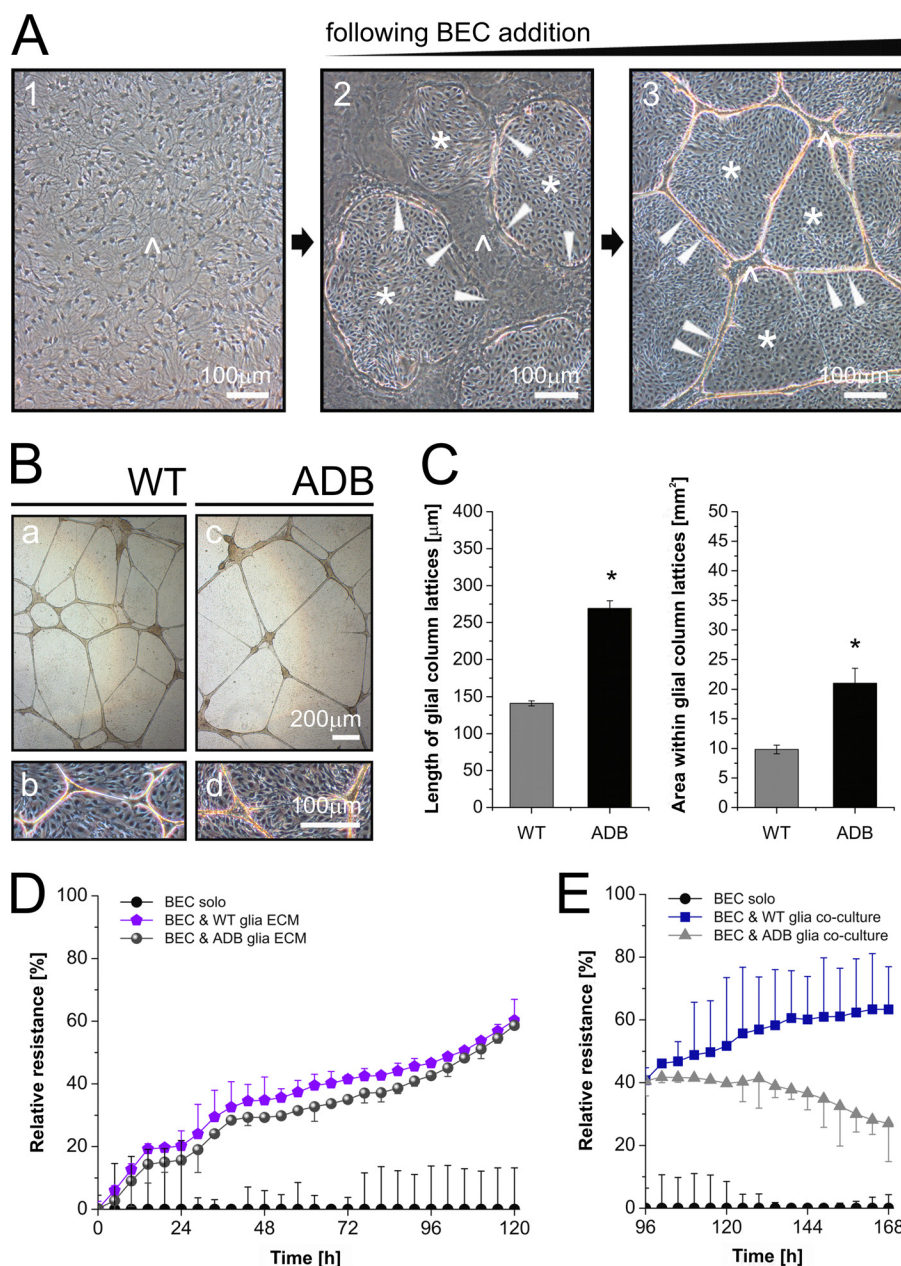
FIGURE 2. **Structural and functional abnormalities in endothelia-ADB astrocyte co-cultures.** *A*, phase-contrast images of morphological developments in BEC-astrocyte co-cultures. *Panel 1*, confluent monolayer of wild-type primary astrocytes (*caret*) is penetrated by BEC added into the culture (*panel 2*). The presence of BEC (*asterisk*) triggers rearrangement of glia into islands (*panel 2*, the *arrows* denote astrocytic island margins) interconnected by thick multicellular glial columns. The size of the islands decreases with time in culture (*panel 3*), whereas the columns elongate and the complexity of their network increases. *B*, comparison of phase-contrast images of BEC co-cultured with wild-type or ADB astrocytes. Control astrocytes (*panels a* and *b*) formed typical arrangements, which were highly reproducible and stable. The ADB glia lattice framework was significantly less complex and fragile (*panels c* and *d*) as shown by statistically significant differences ($p < 0.01$) in morphometric analyses (*C*) where ADB columns were longer and the surface areas in between lattices larger. *D*, normalized ECIS plot (percentage of relative resistance *versus* time) showing endothelial resistance development in BEC cultured on wild-type or ADB astrocyte-derived ECMs (*i.e.* no live cell contact). *E*, relative resistance in BEC co-cultured with either wild-type or ADB astrocytes (live cell-cell contact). Note the significant divergence in ECIS values between cultures containing the two astrocyte types but no difference when glia-derived ECM were used.

(Fig. 2*B*). Surviving columns were extended and sustained by their larger than usual width (Fig. 2). Morphometric measurements confirmed that the BEC/ADB glia columns were indeed fewer than those formed by BEC/WT astrocytes. ADB columns were also significantly longer (albeit brittle), and thus, areas in between lattices were larger (Fig. 2*C*). Electric cell-substrate impedance sensing was used to assess the functional impact of ADB glia in this BBB model. Both direct cell-cell interactions and ECM produced by astrocytes significantly increase imped-

ance (34). Although we found no alteration of the relative values in BEC cultured on ECMs produced by either the wild-type glia or the ADB glia (Fig. 2*D*), there was a dramatic difference in BEC co-cultured with WT *versus* ADB astrocytes (*i.e.* with a direct cell-cell contact) (Fig. 2*E*).

Subsequently, BEC/astrocyte co-cultures were analyzed using immunofluorescence with confocal microscopy. Z-stacks taken through two-dimensional cultures at the points of interface between Kir4.1-positive glial columns and endothelial cells
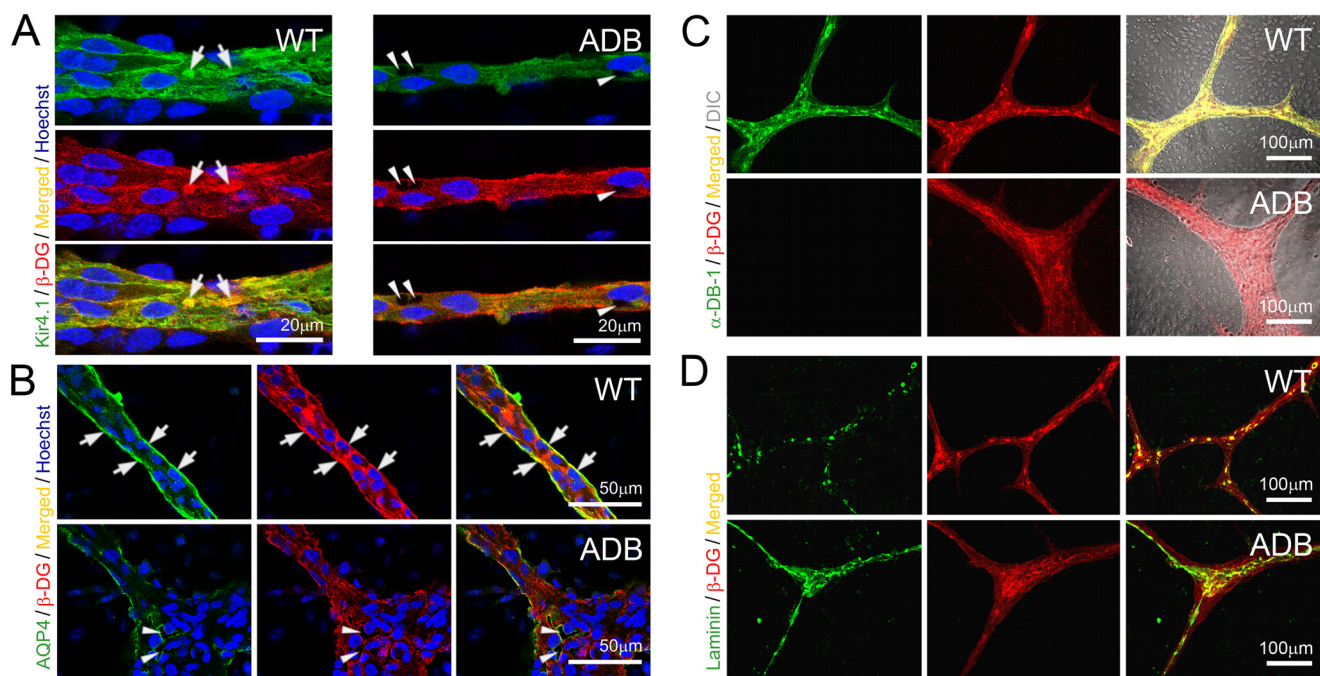
FIGURE 3. **Alterations at glial endfeet in the absence of α-dystrobrevin.** Representative confocal immunofluorescence images were taken under identical settings through glia in BEC/astrocyte co-cultures. *A* and *B*, in ADB co-cultures, analyses revealed vacuolated spaces (*arrowheads*) near the cell attachment points on the basal surface. Staining for Kir4.1 (*A, green*) and AQP4 (*B, green*) revealed significantly decreased expression levels and disruption of normal co-localization of these proteins with β-dystroglycan (*β-DG, red*) of DAP complexes. Note the diffuse distribution and loss of co-localization (*yellow signal, arrows*) in ADB samples (*A* and *B*). This coincided with disruption of the DAP assembly itself in the absence of α-DB (*C*) as shown here by the lack of signal co-localization for β-dystroglycan and its extracellular ligand, laminin (*D*).

showed that ADB astrocytes contained large intracellular vacuoles scattered throughout the cytoplasm (Fig. 3). This abnormality was not present in wild-type cells. Vacuolation could be indicative of a defect in water and/or ion transport. Considering that AQP4 and Kir4.1 channels involved in water/potassium homeostasis are known to be anchored in the cell membrane via specific interactions with DAP (16), we have studied these two proteins. Fluorescence signals for both AQP4 and Kir4.1 in ADB astrocytes were more diffuse and lost from cell membranes (Fig. 3B), which coincided with a lack of co-localization with DAP complexes. Indeed, the lack of co-localization of β-dystroglycan (used as a membrane-associated marker of DAP) and its extracellular ligand, laminin, revealed disruption of the very DAP complexes in ADB astrocytes (Fig. 3, *C* and *D*).

We then analyzed capillary formation in three-dimensional co-culture systems (Fig. 4). In this well established model, BEC and wild-type astrocytes formed well delineated tubular structures with astrocyte contact points being immunopositive for DAP. This regular arrangement was largely lost when ADB glia was used, with cells growing in large, dense clusters (Fig. 4).

Alterations of Both Glial and Endothelial Proteins in the Absence of α-Dystrobrevin—To understand the molecular mechanisms underlying these morphological and functional abnormalities occurring in the absence of α-DB, we have analyzed changes in expression of specific proteins in developing and fully establishing co-cultures (Fig. 5). First, to unequivocally identify cells producing specific proteins, we compared samples from astrocytes and endotheliocytes cultured separately (Fig. 5A). Western blotting of proteins from wild-type astrocytes confirmed significant expression of dystrophin Dp71, but only traces of utrophin (not shown) were found.

There was a significant expression of DAP proteins: dystrobrevins (predominantly α-DB), α- and β-dystroglycans, lower levels of syntrophins, laminin, and Kir4.1, and traces of AQP4. Moreover, astrocytes expressed ZO-1 but no tight junction protein occludin. ADB astrocytes expressed no α-DB but had significantly higher levels of β-DB (Fig. 5A). As expected, BEC cultures expressed tight junction markers ZO-1 and occludin, significant amounts of laminin, and low levels of DAPs such as β-DB, dystroglycans, and syntrophins. Moreover, BEC expressed low levels of Kir4.1 but no α-DB, Dp71, or AQP4 (Fig. 5).

Next, protein samples were taken from co-cultures at time 0 (2 h after the addition of BEC to astrocytes) and 1, 2, 4, 6, and 8 days in co-culture. Western blot analyses showed that there were very significant differences both in temporal expression patterns and in levels of expression of specific DAP-associated proteins as well as endothelial BBB markers between wild-type and ADB co-cultures.

Specifically, glial Kir4.1 potassium channel and endothelial occludin were expressed from the earliest stages in wild-type cultures, but in ADB, the onset of their expressions was delayed by 2–4 days. Expression of AQP4 was also delayed, first appearing at day 6 in wild-type but at day 8 in ADB samples (Fig. 5A). Moreover, expression levels of these three proteins as well as of laminin were significantly reduced in ADB co-cultures at all time points analyzed (Fig. 5A). Interestingly, time course analysis showed that expression of the Dp71 dystrophin isoform decreased gradually with days in culture, with a dramatic drop between days 4 and 6 and disappearance at day 8 of culture in both wild-type and ADB samples (Fig. 5A). Nevertheless, Dp71 levels were reduced at all time points in ADB co-cultures. As
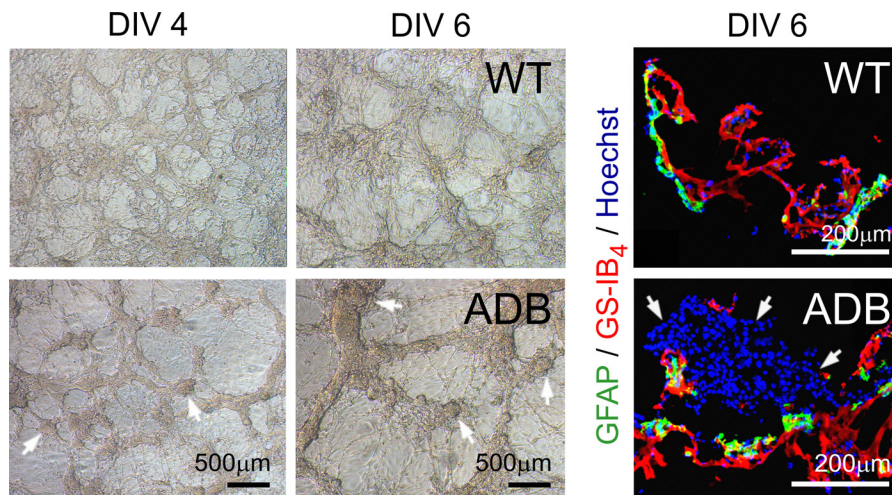
FIGURE 4. **Malformation of three-dimensional assemblies of BEC co-cultured with ADB glia.** Wild-type astrocytes induced the formation of well delineated tubular endothelial structures clearly evident at day 4. Confocal microscopy analyses at day 6 confirmed that GFAP-labeled wild-type astrocytes were in contact with the GS-IB$_4$-labeled endothelial tubes, whereas ADB astrocytes did not support the endothelial tubulogenesis. Here, remnants of cyst-like structures that initiated the early branching of endothelial tubes were still fairly intact at days 4 and 6. Although contacts between ADB astrocytes and endothelial tube-like structures were made, the latter appeared unusually thick. *Left-side panels*, phase-contrast images of three-dimensional cultures of glia with BEC. In the *WT panel*, note the fine, dense connections with intricate vessel-like structures at day 4 *in vitro* (*DIV 4*), becoming more pronounced and networked by day 6. In the *ADB panel*, note fewer, broader, and discontinuous structures and cysts (*arrows*), a sign that early vessel development is evident. By day 6, some cysts remained, and vessel assemblies broadened. *Right-hand side panels*, representative confocal images in three-dimensional co-cultures. BEC and wild-type astrocytes formed well defined tubular structures, with astrocytes (positive for GFAP, *green*) arranged in a continuous sheath along and around the endothelial vessel-like assemblies (stained with GS-IB$_4$, *red*). In the presence of ADB glia, these orderly arrangements were lost, and cells have grown in large, dense clusters (*arrows*).

expected, expression patterns of specific dystrophin-associated proteins were also altered, with overexpression of β-DB in the absence of its α-DB and lower levels of α- and β-dystroglycans (Fig. 5*A*). Moreover, AQP4 multimerizes into orthogonal arrays of particles (OAP), a supramolecular assembly that is important for polarization of AQP4 subunits and water movement through pores (37). Blue native-PAGE analyses (Fig. 5*B*) revealed that ADB astrocytes failed to form OAP. As expected, in wild-type cell cultures, these assemblies were formed both in co-cultures with BEC and following pretreatment with laminin (28).

Absence of α-Dystrobrevin Results in Alterations of AQP4 and Kir4.1 and Water Retention in Brains in Situ—Considering the altered expressions of AQP4 and Kir4.1 in ADB astrocytes, we examined distributions of these proteins in brains *in situ*. Immunofluorescent confocal analyses of cellular localizations of these proteins revealed very specific alterations (Fig. 6, *A* and *B*). In normal brains, AQP4 and Kir4.1 were clearly located to the astrocytic endfeet, in close contact with blood vessel endothelia. However, in α-DB-deficient brains, both were dislodged from the endfeet, and instead, increased diffused signal was found in astrocyte cell bodies (Fig. 6, *A* and *B*). Western blotting showed that these differences were caused by mislocalization of AQP4 and Kir4.1 rather than changes in expression as there was no significant decrease of protein levels in ADB brains (Fig. 6*C*). It was also the case for syntrophin, the DAP protein tethering AQP4 and Kir4.1 to dystrobrevin (Fig. 6*C*). Moreover, this dislocation of water/ion channels coincided with significantly increased base-line water content in ADB mice hemispheres than in WT controls ($p < 0.005$) despite the total brain mass being higher in WT brains (Fig. 6*D*).

Glial Vacuolation, Progressive Brain Edema, and Neurovascular Unit Damage in the Absence of α-DB—Taking into account the AQP4 and Kir4.1 abnormalities, increased perme-

ability of ADB capillaries, and brain water retention, we have examined young and old age-matched brains morphologically. Although analysis of H&E-stained sections of 3-month-old brains (used in all previous experiments) confirmed no discernible differences, electron microscopy revealed some glial endfeet vacuolation in ADB samples. Furthermore, H&E and EM in aged (18-month-old) ADB samples revealed spongiform degeneration and glial endfeet edema. Tissue spongiosis was severe, particularly in the Ammon horn, the dentate gyrus and in the cerebellum, affecting brain parenchyma, whereas neurons were preserved (Fig. 7*A*). In the EM, tissue edema was not restricted to astrocyte endfeet but extended beyond those, destroying neighboring neuropil and distorting the capillary lumen (Fig. 7*B*). Endothelial cells showed signs of damage with numerous pinocytotic vesicles in the cytoplasm, microvilli on the luminal surface, and tight junction abnormalities. The latter could be linked to thickened basement membranes and apparent hyperplasia (multilayered endothelium) and therefore decreased vessel lumens. Neurons and pericytes of ADB brains also showed signs of damage, and thus, α-DB deficiency affects the entire neurovascular unit. Importantly, analysis of 18-month-old dystrophic (mdx^{βgeo}) brains revealed similar abnormalities.[4] In contrast, WT ultrastructure, albeit showing features typical for aged brains, was otherwise normal.

DISCUSSION

Although BBB relies on the properties of brain endothelial cells, growing data indicate that glia and pericytes of the neurovascular unit are essential for BBB function in BEC. These interactions involve secreted factors (38) and extracellular matrix and cell-cell interactions. Dystrophin absence results in

---

[4] C. F. Lien, M. Frontczak-Baniewicz, B. Zablocka, and D. C. Górecki, manuscript in preparation.
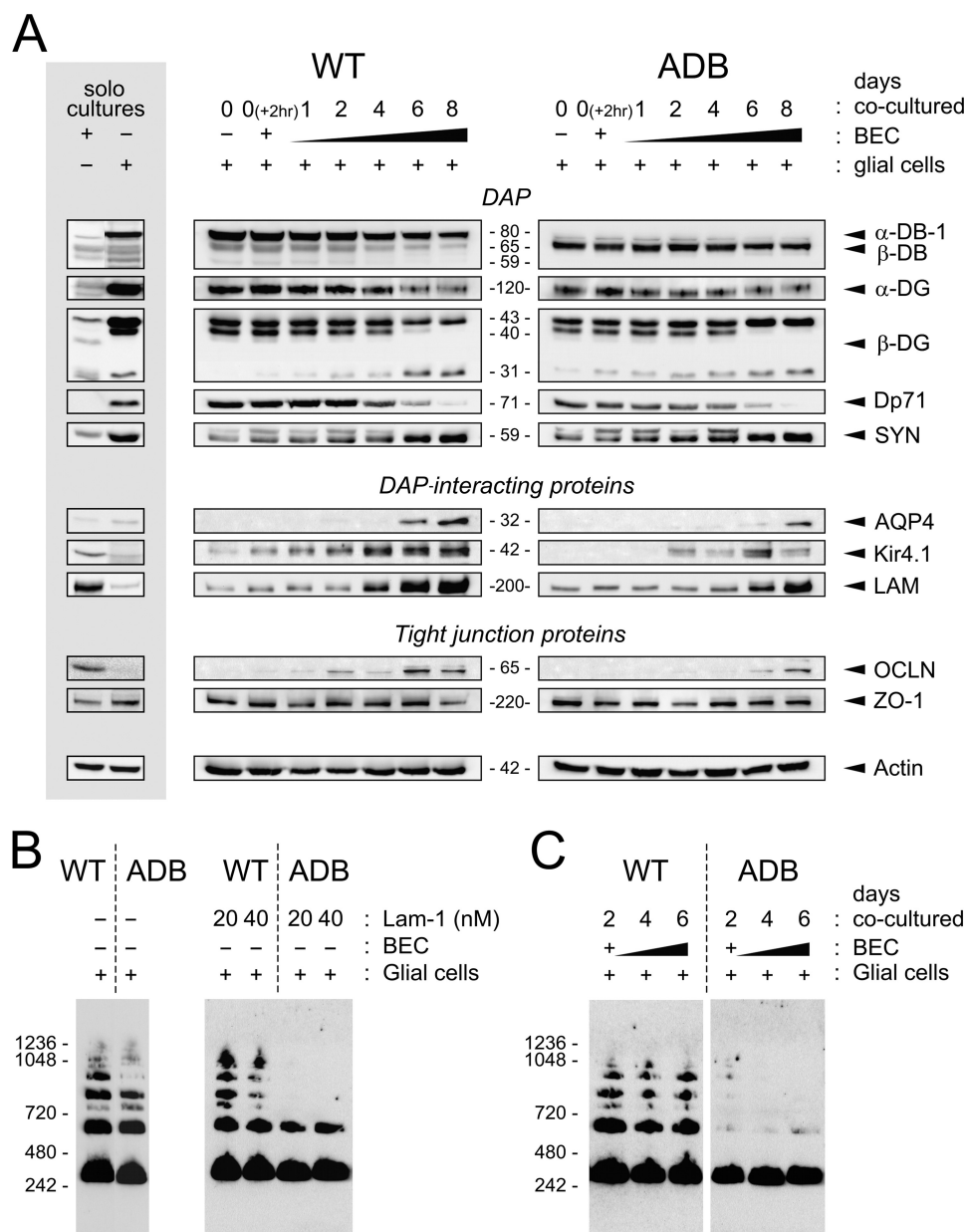
FIGURE 5. **Abnormalities in expression and assembly patterns of glial and endothelial proteins in ADB co-cultures.** *A*, representative immunoblots of protein extracts are shown. In solo cultures, BEC cultured alone expressed ZO-1, occludin (*OCLN*), low levels of β-DB, dystroglycans (*DG*), syntrophins (*SYN*), and laminin (*LAM*). In astrocytes alone, dystrobrevins, dystroglycans, syntrophins, dystrophin Dp71, and ZO-1 were found. Molecular mass (kDa) of each protein is indicated. Actin was used as a control for equal protein loading. Immunoblots of protein extracts from co-cultures of BEC with WT or ADB astrocytes over 8 days in culture show dystrophin and DAPs, DAP-interacting proteins, and BBB markers. There were significant delays in temporal expression patterns and in levels of expression of AQP4, laminin, and Kir4.1 in ADB co-cultures. Expression of dystrophin Dp71 was lower in ADB, and the time course analysis showed gradual decrease of Dp71 levels from day 4 onwards in both control and ADB samples. Expression of BBB marker occludin was detectable from day 2 in wild-type cultures, but in ADB samples, it was noticeable from day 6 only. *B* and *C*, blue native-PAGE analysis of OAP formation. AQP4 immunoblots following blue native-PAGE of cell lysates of wild-type and ADB astrocytes either pretreated with increasing concentrations of laminin-1 (20 and 40 nM) (*B*) or co-cultured with BEC (*C*). Under both conditions, ADB astrocytes failed to form OAP, in clear contrast to the wild-type cells.

leaky BBB (9) (Fig. 1). However, the mechanism of this abnormality is unclear, especially as dystrophin is not expressed in BEC forming the BBB. This indicates an indirect effect of the dystrophin absence and points to abnormality occurring specifically in astrocytic glial endfeet. Astrocytes, unlike brain BEC and pericytes, contain a specific set of dystrophin-associated proteins. The results of this study show that one member of the glial DAP, α-dystrobrevin, is vital for proper BBB formation and function. Its absence in ADB knock-out mice, even in the presence of dystrophins, causes profound blood-brain barrier

abnormality. This is an important result as it uncovers one of the still poorly understood molecular mechanisms functioning at the cell-cell interface between endothelia and glia. In this context, α-dystrobrevin emerges as a rare example of a glial protein with a specific role in maintaining BBB function. Bearing in mind that α-DB is an entirely intracellular protein, the mechanisms that could explain its influence over endothelial cells must include indirect interactions. Dystrobrevin links dystrophin/utrophin, dystroglycan, and the syntrophin families of proteins. This interaction is reciprocal as proper localization of
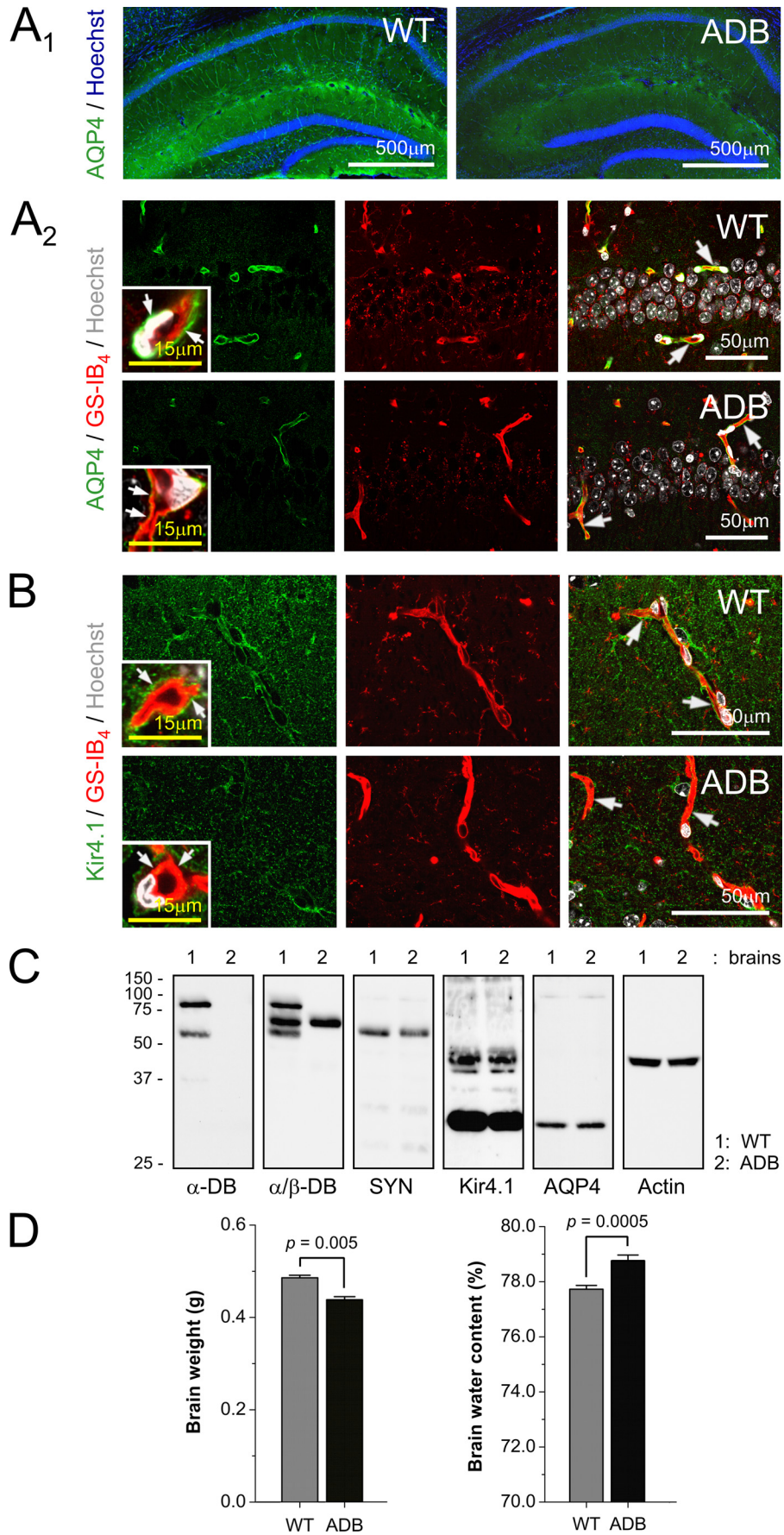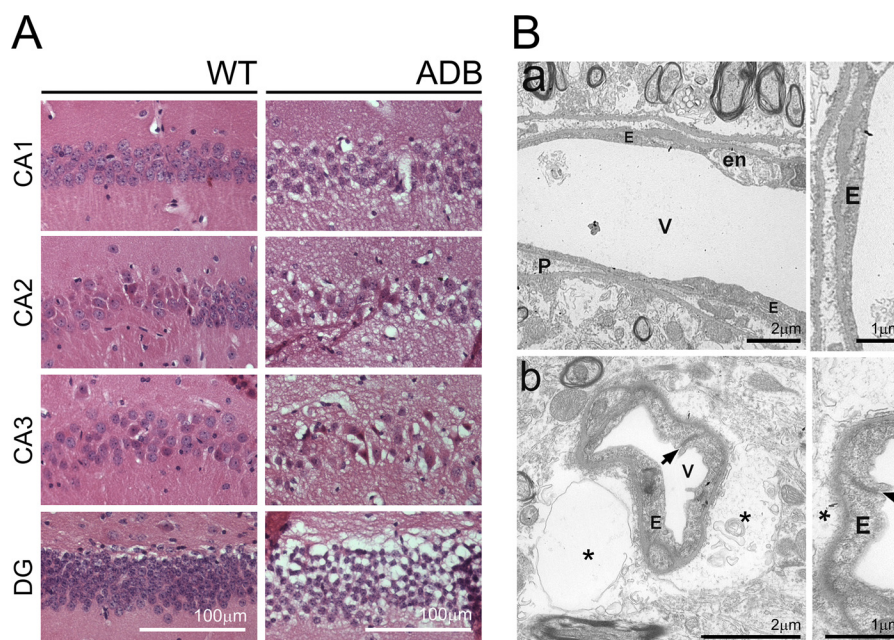
FIGURE 7. **Absence of α-DB causes spongiform neurodegeneration and progressive brain edema.** *A*, H&E staining of hippocampal areas of 18-month-old WT and ADB mice showing massive spongiosis evident in the parenchyma of the pyramidal cell layer, particularly regions CA2 and CA3, and in the granule cell layer of the dentate gyrus (*DG*) in ADB brains. *B*, electron microscopic images of brain cortex of WT (*panel a*) and ADB (*panel b*) mice. *Panel a*, regular capillary vessel (*V*) with pericytes (*P*) and endothelium (*E*) characterized by necrotic features in some cells (*en*), typically associated with aging. *Panel b*, capillary vessel in ADB cortex surrounded by vast astrocytic edema (*asterisk*). Endothelial cell cytoplasm is rich in pinocytotic vesicles. The *arrow* points to an improper tight junction between endothelial cells.

α-dystrobrevin requires α-syntrophin (39, 40). Resulting DAP scaffolds interact with ECM components (*e.g.* laminin) and serve to anchor a further set of proteins, including receptors and channels (41, 42). We have shown that α-DB absence produced rearrangements of DAP components resulting in a secondary decrease or loss of their interacting proteins. Morphological disarrangements that we observed in ADB astrocyte-BEC co-cultures could be caused by abnormalities in cell attachments due to decreased levels of laminin and dystroglycan, in a mechanism analogous to dystrophic muscle damage. However, as ADB astrocytes *in vitro* and *in vivo* contained large intracellular vacuoles, this could indicate defects in water and/or ion transport. Therefore, a different mechanism could be envisaged; laminin, dystroglycan, and syntrophin have a role in Kir4.1 potassium and AQP4 water channel aggregation and localization at glial endfeet (42, 43, 44), and these two proteins are important for ion and water transport (see below). Our data advance our understanding of these astrocyte specializations by demonstrating that α-DB is a key scaffolding protein for AQP4 and Kir4.1 at glial endfeet. Consequently, morphological malformations in co-cultures *in vitro*, increased BBB permeability, and progressive brain edema in ADB brains *in vivo* could result from abnormalities of water and ion homeostasis in astrocytes and at the glia-BEC interface.

Astrocytic perivascular endfeet cover the vessel wall completely (45) and thus must play a part in the exchange of water and solutes between blood and brain. The presence of AQP4 and Kir4.1 at glial endfeet is of vital importance for ion and water homeostasis. Active neurons release K^+ and water. K^+ is taken up by glial processes surrounding neurons and then released at the distant perivascular endfeet via the potassium spatial buffer mechanism (2). The net ion gain results in osmotic water uptake, and the co-localization of AQP4 water channels in endfeet is essential for redistribution of excess water (46, 47). Disruptions of glial endfeet assembly impair these functions and could lead to osmotic opening of tight junctions in response to changes in cell volume (48). If that were the case, any disruption to the DAP complex should produce alterations of BBB functions. Indeed, mdx dystrophic mice, α-syntrophin-null mice and, as shown here, α-dystrobrevin-null mice all show such abnormalities (10, 49, 50).

The blood-brain barrier in the higher vertebrates is formed by endothelial cells. However, in lower organisms (invertebrates up to the elasmobranch fish), it is created by glia. Evidently, during evolution, the BBB shifted from the glial to endothelial compartment (51). It is, therefore, not surprising that intricate interactions of BEC with glia influence the BBB properties in mammals (2, 7, 52). Moreover, there is increasing evi-

FIGURE 6. **Abnormal localization of Kir4.1 and AQP4 in ADB brains.** *A* and *B*, representative micrographs of immunolocalizations from AQP4 (*A*) and Kir4.1 (*B*) in mouse brains. *A₁*, in the small magnification view of hippocampus, AQP4 staining (*green*) delineates capillaries in the wild-type brains but not in ADB brains. Confocal co-localizations of AQP4 (*A₂, green*) and Kir4.1 (*B, green*) with GS-IB₄-labeled endothelia (*A₂ and B, red*) show AQP4 and Kir4.1 signals located in close proximity to endothelia (*yellow, arrows*) in WT but not ADB brains. *Inset,* Larger magnification image confirms that this corresponds with the loss of signals from ADB astrocytic endfeet (*arrows*). Hoechst (*blue/white*) was used as a nuclear counterstain, where indicated. *C*, representative immunoblots of brain protein extracts demonstrate the relative levels of AQP4, Kir4.1, syntrophin (*SYN*), and β-DB in the absence of α-DB. Actin was used as a control for equal protein loading. *D*, total brain mass and base-line water content analyses showed significant differences ($p < 0.005$ and $p < 0.0005$) between age-matched 3-month-old WT and ADB brains.

dence that dysfunctions at the abluminal surface of BEC in contact with astrocytes (1, 2) and endfeet abnormalities (53) may contribute to BBB damage in several neuropathologies. Specifically, redistribution of AQP4 in perivascular endfeet coincides with increased BBB permeability in glioblastomas or with brain edema (54). However, we are only beginning to understand the exact molecular mechanisms functioning at the interface between endothelial and glial cells. Our data provide a new insight into these interactions and introduce α-dystrobrevin and the dystrophin-associated protein complex as important players in this process.

It needs to be confirmed whether these abnormalities occur in human brains. As dystrophinopathies lead to premature death of young adults due to muscle failure, no data on aged dystrophic brains exist. However, the impact of α-DB mutations might be greater in humans than what has been observed here in mice. Due to lineage-specific mutations in the murids (55), the mouse brain has fewer than half of the isoforms found in the human brain (56). The human α-DB gene encodes three distinct syntrophin-binding sites, resulting in a greatly enhanced functional repertoire. Therefore, α-DB absence in humans might be significantly more damaging.

REFERENCES

1. Zlokovic, B. V. (2008) The blood-brain barrier in health and chronic neurodegenerative disorders. *Neuron* **57,** 178–201
2. Abbott, N. J., Patabendige, A. A., Dolman, D. E., Yusof, S. R., and Begley, D. J. (2010) Structure and function of the blood-brain barrier. *Neurobiol. Dis.* **37,** 13–25
3. Giaume, C., Koulakoff, A., Roux, L., Holcman, D., and Rouach, N. (2010) Astroglial networks: a step further in neuroglial and gliovascular interactions. *Nat. Rev. Neurosci.* **11,** 87–99
4. Liebner, S., and Engelhardt, B. (2005) in *The Blood-Brain Barrier and Its Microenvironment: Basic Physiology to Neurological Disease* (DeVries, E., and Prat, A., eds) pp. 1–25, New York: Taylor & Francis
5. Abbott, N. J., Rönnbäck, L., and Hansson, E., (2006) Astrocyte-endothelial interactions at the blood-brain barrier. *Nat. Rev. Neurosci.* **7,** 41–53
6. Haseloff, R. F., Blasig, I. E., Bauer, H. C., and Bauer, H. (2005) In search of the astrocytic factor(s) modulating blood-brain barrier functions in brain capillary endothelial cells *in vitro. Cell. Mol. Neurobiol.* **25,** 25–39
7. Nedergaard, M., Ransom, B., and Goldman, S. A. (2003) New roles for astrocytes: redefining the functional architecture of the brain. *Trends Neurosci.* **26,** 523–530
8. del Zoppo, G. J., and Milner, R. (2006) Integrin-matrix interactions in the cerebral microvasculature. *Arterioscler. Thromb. Vasc. Biol.* **26,** 1966–1975
9. Nico, B., Roncali, L., Mangieri, D., and Ribatti, D. (2005) Blood-brain barrier alterations in MDX mouse, an animal model of the Duchenne muscular dystrophy. *Curr. Neurovasc. Res.* **2,** 47–54
10. Vajda, Z., Pedersen, M., Füchtbauer, E. M., Wertz, K., Stødkilde-Jørgensen, H., Sulyok, E., Dóczi, T., Neely, J. D., Agre, P., Frøkiaer, J., and Nielsen, S. (2002) Delayed onset of brain edema and mislocalization of aquaporin-4 in dystrophin-null transgenic mice. *Proc. Natl. Acad. Sci. U.S.A.* **99,** 13131–13136
11. Lien, C. F., Hazai, D., Yeung, D., Tan, J., Füchtbauer, E. M., Jancsik, V., and Górecki, D. C. (2007) Expression of α-dystrobrevin in blood-tissue barriers: sub-cellular localisation and molecular characterisation in normal and dystrophic mice. *Cell Tissue Res.* **327,** 67–82
12. Lien, C. F, Vlachouli, C., Blake, D. J., Simons, J. P., and Górecki, D. C. (2004) Differential spatio-temporal expression of α-dystrobrevin-1 during mouse development. *Gene Expr. Patterns* **4,** 583–593
13. Blake, D. J., Nawrotzki, R., Loh, N. Y., Górecki, D. C., and Davies, K. E. (1998) β-Dystrobrevin, a member of the dystrophin-related protein family. *Proc. Natl. Acad. Sci. U.S.A.* **95,** 241–246
14. Hazai, D., Lien, C. F., Hajós, F., Halasy, K., Górecki, D. C., and Jancsik, V. (2008) Synaptic α-dystrobrevin: localization of a short α-dystrobrevin isoform in melanin-concentrating hormone neurons of the hypothalamus. *Brain Res.* **1201,** 52–59
15. Newey, S. E., Howman, E. V., Ponting, C. P., Benson, M. A., Nawrotzki, R., Loh, N. Y., Davies, K. E., and Blake, D. J. (2001) Syncoilin, a novel member of the intermediate filament superfamily that interacts with α-dystrobrevin in skeletal muscle. *J. Biol. Chem.* **276,** 6645–6655
16. Rees, M. L., Lien, C. F., and Górecki, D. C. (2007) Dystrobrevins in muscle and non-muscle tissues. *Neuromuscul. Disord.* **17,** 123–134
17. Grady, R. M., Grange, R. W., Lau, K. S., Maimone, M. M., Nichol, M. C., Stull, J. T., and Sanes, J. R. (1999) Role for α-dystrobrevin in the pathogenesis of dystrophin-dependent muscular dystrophies. *Nat. Cell Biol.* **1,** 215–220
18. Zea-Aragón, Z., Terada, N., Ohno, N., Fujii, Y., Baba, T., and Ohno, S. (2004) Effects of anoxia on serum immunoglobulin and albumin leakage through blood-brain barrier in mouse cerebellum as revealed by cryotechniques. *J. Neurosci. Methods* **138,** 89–95
19. Zhao, L., Moos, M. P., Gräbner, R., Pédrono, F., Fan, J., Kaiser, B., John, N., Schmidt, S., Spanbroek, R., Lötzer, K., Huang, L., Cui, J., Rader, D. J., Evans, J. F., Habenicht, A. J., and Funk, C. D. (2004) The 5-lipoxygenase pathway promotes pathogenesis of hyperlipidemia-dependent aortic aneurysm. *Nat. Med.* **10,** 966–973
20. *Gräbner, R., Lötzer, K., Döpping, S., Hildner, M.,* Radke, D., Beer, M., Spanbroek, R., Lippert, B., Reardon, C. A., Getz, G. S., Fu, Y. X., Hehlgans, T., Mebius, R. E., van der Wall, M., Kruspe, D., Englert, C., Lovas, A., Hu, D., Randolph, G. J., Weih, F., and Habenicht, A. J. (2009) Lymphotoxin β receptor signaling promotes tertiary lymphoid organogenesis in the aorta adventitia of aged *ApoE*$^{-/-}$ mice. *J. Exp. Med.* **206,** 233–248
21. Haj-Yasein, N. N., Vindedal, G. F., Eilert-Olsen, M., Gundersen, G. A., Skare, Ø., Laake, P., Klungland, A., Thorén, A. E., Burkhardt, J. M., Ottersen, O. P., and Nagelhus, E. A. (2011) Glial-conditional deletion of aquaporin-4 (Aqp4) reduces blood-brain water uptake and confers barrier function on perivascular astrocyte endfeet. *Proc. Natl. Acad. Sci. U.S.A.* **108,** 17815–17820
22. Marriott, D. R., Hirst, W. D., and Ljungberg, M. C. (1995) in *Neural Cell Culture: A Practical Approach* (Cohen, J., and Wilkin, G. P., eds) pp. 85–96, Oxford University Press Inc., New York
23. Saura, J. (2007) Microglial cells in astroglial cultures: a cautionary note. *J. Neuroinflammation* **4,** 26
24. Crocker, S. J., Frausto, R. F., Whitton, J. L., and Milner, R. (2008) A novel method to establish microglia-free astrocyte cultures: comparison of matrix metalloproteinase expression profiles in pure cultures of astrocytes and microglia. *Glia* **56,** 1187–1198
25. Saura, J., Tusell, J. M., and Serratosa, J. (2003) High-yield isolation of murine microglia by mild trypsinization. *Glia* **44,** 183–189
26. Brown, R. C., Morris, A. P., and O'Neil, R. G. (2007) Tight junction protein expression and barrier properties of immortalized mouse brain microvessel endothelial cells. *Brain Res.* **1130,** 17–30
27. Hagberg, C. E., Falkevall, A., Wang, X., Larsson, E., Huusko, J., Nilsson, I., van Meeteren, L. A., Samen, E., Lu, L., Vanwildemeersch, M., Klar, J., Genove, G., Pietras, K., Stone-Elander, S., Claesson-Welsh, L., Ylä-Herttuala, S., Lindahl, P., and Eriksson, U. (2010) Vascular endothelial growth factor B controls endothelial fatty acid uptake. *Nature* **464,** 917–921
28. Noël, G., Stevenson, S., and Moukhles, H. (2011) A high throughput screen identifies chemical modulators of the laminin-induced clustering of dystroglycan and aquaporin-4 in primary astrocytes. *PLoS One* **6,** e17559
29. Imamura, M., and Ozawa, E. (1998) Differential expression of dystrophin isoforms and utrophin during dibutyryl-cAMP-induced morphological differentiation of rat brain astrocytes. *Proc. Natl. Acad. Sci. U.S.A.* **95,** 6139–6144

30. Ment, L. R., Stewart, W. B., Scaramuzzino, D., and Madri, J. A. (1997) An *in vitro* three-dimensional coculture model of cerebral microvascular angiogenesis and differentiation. *In Vitro Cell. Dev. Biol. Anim.* **33,** 684–691

31. Chow, J., Ogunshola, O., Fan, S. Y., Li, Y., Ment, L. R., and Madri, J. A. (2001) Astrocyte-derived VEGF mediates survival and tube stabilization of hypoxic brain microvascular endothelial cells *in vitro*. *Brain Res. Dev. Brain Res* **130,** 123–132

32. Al Ahmad, A., Taboada, C. B., Gassmann, M., and Ogunshola, O. O. (2011) Astrocytes and pericytes differentially modulate blood-brain barrier characteristics during development and hypoxic insult. *J. Cereb. Blood Flow Metab.* **31,** 693–705

33. Lien, C. F., Molnár, E., Toman, P., Tsibouklis, J., Pilkington, G. J., Górecki, D. C., and Barbu, E. (2012) *In vitro* assessment of alkylglyceryl-functionalized chitosan nanoparticles as permeating vectors for the blood-brain barrier. *Biomacromolecules* **13,** 1067–1073

34. Hartmann, C., Zozulya, A., Wegener, J., and Galla, H. J. (2007) The impact of glia-derived extracellular matrices on the barrier function of cerebral endothelial cells: an *in vitro* study. *Exp. Cell Res.* **313,** 1318–1325

35. Sorbo, J. G., Moe, S. E., Ottersen, O. P., and Holen, T. (2008) The molecular composition of square arrays. *Biochemistry* **47,** 2631–2637

36. Yoder, E. J. (2002) Modifications in astrocyte morphology and calcium signaling induced by a brain capillary endothelial cell line. *Glia* **38,** 137–145

37. Wolburg, H., Wolburg-Buchholz, K., Fallier-Becker, P., Noell, S., and Mack, A. F. (2011) Structure and functions of aquaporin-4-based orthogonal arrays of particles. *Int. Rev. Cell Mol. Biol.* **287,** 1–41

38. Alvarez, J. I., Dodelet-Devillers, A., Kebir, H., Ifergan, I., Fabre, P. J., Terouz, S., Sabbagh, M., Wosik, K., Bourbonnière, L., Bernard, M., van Horssen, J., de Vries, H. E., Charron, F., and Prat, A. (2011) The Hedgehog pathway promotes blood-brain barrier integrity and CNS immune quiescence. *Science* **334,** 1727–1731

39. Bragg, A. D., Amiry-Moghaddam, M., Ottersen, O. P., Adams, M. E., and Froehner, S. C. (2006) Assembly of a perivascular astrocyte protein scaffold at the mammalian blood-brain barrier is dependent on α-syntrophin. *Glia* **53,** 879–890

40. Bragg, A. D., Das, S. S., and Froehner, S. C. (2010) Dystrophin-associated protein scaffolding in brain requires α-dystrobrevin. *Neuroreport* **21,** 695–699

41. Connors, N. C., Adams, M. E., Froehner, S. C., and Kofuji, P. (2004) The potassium channel Kir4.1 associates with the dystrophin-glycoprotein complex via α-syntrophin in glia. *J. Biol. Chem.* **279,** 28387–28392

42. Peters, M. F., O'Brien, K. F., Sadoulet-Puccio, H. M., Kunkel, L. M., Adams, M. E., and Froehner, S. C. (1997) β-Dystrobrevin, a new member of the dystrophin family: identification, cloning, and protein associations. *J. Biol. Chem.* **272,** 31561–31569

43. Guadagno, E., and Moukhles, H. (2004) Laminin-induced aggregation of the inwardly rectifying potassium channel, Kir4.1, and the water-permeable channel, AQP4, via a dystroglycan-containing complex in astrocytes. *Glia* **47,** 138–149

44. Neely, J. D., Amiry-Moghaddam, M., Ottersen, O. P., Froehner, S. C., Agre, P., and Adams, M. E. (2001) Syntrophin-dependent expression and localization of Aquaporin-4 water channel protein. *Proc. Natl. Acad. Sci. U.S.A.* **98,** 14108–14113

45. Mathiisen, T. M., Lehre, K. P., Danbolt, N. C., and Ottersen, O. P. (2010) The perivascular astroglial sheath provides a complete covering of the brain microvessels: an electron microscopic 3D reconstruction. *Glia* **58,** 1094–1103

46. Bloch, O., and Manley, G. T. (2007) The role of aquaporin-4 in cerebral water transport and edema. *Neurosurg. Focus* **22,** E3

47. Reichenbach, A., Wurm, A., Pannicke, T., Iandiev, I., Wiedemann, P., and Bringmann, A. (2007) Müller cells as players in retinal degeneration and edema. *Graefes. Arch. Clin. Exp. Ophthalmol.* **245,** 627–636

48. Simard, M., and Nedergaard, M. (2004) The neurobiology of glia in the context of water and ion homeostasis. *Neuroscience* **129,** 877–896

49. Nico, B., Frigeri, A., Nicchia, G. P., Corsi, P., Ribatti, D., Quondamatteo, F., Herken, R., Girolamo, F., Marzullo, A., Svelto, M., and Roncali, L. (2003) Severe alterations of endothelial and glial cells in the blood-brain barrier of dystrophic mdx mice. *Glia* **42,** 235–251

50. Nico, B., Paola Nicchia, G., Frigeri, A., Corsi, P., Mangieri, D., Ribatti, D., Svelto, M., and Roncali, L. (2004) Altered blood-brain barrier development in dystrophic MDX mice. *Neuroscience* **125,** 921–935

51. Banerjee, S., and Bhat, M. A. (2007) Neuron-glial interactions in blood-brain barrier formation. *Annu. Rev. Neurosci.* **30,** 235–258

52. Takano, T., Tian, G. F., Peng, W., Lou, N., Libionka, W., Han, X., and Nedergaard, M. (2006) Astrocyte-mediated control of cerebral blood flow. *Nat. Neurosci.* **9,** 260–267

53. Wilcock, D. M., Vitek, M. P., and Colton, C. A. (2009) Vascular amyloid alters astrocytic water and potassium channels in mouse models and humans with Alzheimer's disease. *Neuroscience* **159,** 1055–1069

54. Amiry-Moghaddam, M., Frydenlund, D. S., and Ottersen, O. P. (2004) Anchoring of aquaporin-4 in brain: molecular mechanisms and implications for the physiology and pathophysiology of water transport. *Neuroscience* **129,** 999–1010

55. Böhm, S. V., Constantinou, P., Tan, S., Jin, H., and Roberts, R. G. (2009) Profound human/mouse differences in α-dystrobrevin isoforms: a novel syntrophin-binding site and promoter missing in mouse and rat. *BMC Biol.* **7,** 85

56. Newey, S. E., Benson, M. A., Ponting, C. P., Davies, K. E., and Blake, D. J. (2000) Alternative splicing of dystrobrevin regulates the stoichiometry of syntrophin binding to the dystrophin protein complex. *Curr. Biol.* **10,** 1295–1298